EurJIC European Journal of Inorganic Chemistry
ChemPubSoc Europe

FULL PAPER

DOI:10.1002/ejic.201201499

Incorporation of Hydrogen-Bonding Functionalities into the Second Coordination Sphere of Iron-Based Water-Oxidation Catalysts

Wesley A. Hoffert,[a] Michael T. Mock,[a] Aaron M. Appel,[a] and Jenny Y. Yang*[b][‡]

Keywords: Homogeneous catalysis / Water splitting / Iron / Ligand effects / Proton transport

Energy storage and conversion schemes based on environmentally benign chemical fuels will require the discovery of faster, cheaper, and more robust catalysts for the oxygen-evolution reaction (OER). Although the incorporation of pendant bases into molecular catalysts for hydrogen production and utilization has led to enhanced turnover frequencies, the analogous incorporation of pendant bases into molecular catalysts for water oxidation has received little attention. Herein, the syntheses, structures, and catalytic activities of new iron complexes with pendant bases are reported. Of these new complexes, $[Fe(\mathbf{L^1})]^{2+}$ {$\mathbf{L^1}$ = *N*,*N*′-dimethyl-*N*,*N*′-bis(pyridazin-3-ylmethyl)ethane-1,2-diamine} is the most active catalyst. Initial turnover frequencies of 141 and 24 h^{-1} were measured by using ceric ammonium nitrate at pH 0.7 and sodium periodate at pH 4.7, respectively. These results suggest that the incorporation of pendant bases into molecular catalysts for water oxidation might be an effective strategy that can be considered in the development of new catalysts for the OER, but will require the careful balance of many factors.

Introduction

The successful implementation of a carbon-neutral energy infrastructure hinges on many factors, including the discovery of earth-abundant catalysts capable of transforming readily available materials into chemical fuels for energy storage to compensate for the intermittent nature of renewable energy sources. Whereas there are a variety of choices for reduction of substrates to fuels, they all require a corresponding oxidative half-reaction to generate the necessary protons and reducing equivalents. In this regard, catalyzing the 4 e^-, 4H^+ oxygen-evolution reaction [OER; Equation (1)] has been a focus of many research groups, and an increasing emphasis has been placed on the use of first-row transition-metal complexes owing to their relatively low cost and rich redox chemistry.

$$2H_2O \rightarrow O_2 + 4H^+ + 4e^- \quad (1)$$

Several crucial design principles must be considered for such complexes, not least of which is the use of oxidatively robust supporting ligands on account of the high standard potential for Equation (1) ($E°$ = +1.23 V versus NHE). One approach has been to study metal–oxo cluster complexes as synthetic models of the oxygen-evolving Mn_4Ca complex in photosystem II.[1,2] Mayer et al. have recently discovered that $[Cu(bpy)]^{2+}$ (bpy = 2,2′-bipyridyl) complexes can oxidize water electrocatalytically under highly basic conditions.[3] Costas and co-workers have also reported a family of *cis*-$[Fe^{II}(N_4)]^{2+}$ complexes that serve as efficient homogeneous water-oxidation catalysts in which N_4 is a neutral, tetradentate ligand (Figure 1, a).[4] In a related experiment, Arnold et al. have also demonstrated that $[M^{II}(tpa)]^{2+}$ [M = Mn, Fe, Co, Cu; tpa = tris(2-pyridylmethyl)amine] complexes also catalyze the reverse reaction, O_2-reduction.[5] Considering the 4 e^-, 4H^+ transformation required for the OER, the coupling of proton- and electron-transfer events is critical for effective proton management and can lead to improved reaction kinetics and lower thermodynamic barriers in the catalytic cycle. The benefit of proton relays for H^+ reduction and H_2 oxidation has been extensively studied,[6] and this design feature was recently extended to O_2-reduction catalysts by Mayer and co-workers.[7] However, the incorporation of pendant-base functionality into the second coordination sphere of catalysts for water oxidation is a strategy that has received comparatively little attention. Herein, we define the second coordination sphere as ligand-supported chemical substituents that can directly interact with metal-bound substrates (see Figure 1, b).

[a] Pacific Northwest National Laboratory,
Richland, WA, 99352, USA
http://www.pnnl.gov/
[b] Joint Center for Artificial Photosynthesis, California Institute of Technology,
Pasadena, CA, 91125, USA
Homepage: http://solarfuelshub.org/
[‡] Current address: Department of Chemistry, University of California-Irvine, 1102 Natural Sciences II,
Irvine, CA, 92697, USA
Homepage: http://www.chem.uci.edu/people/jenny-yang/
Supporting information for this article is available on the WWW under http://dx.doi.org/10.1002/ejic.201201499.

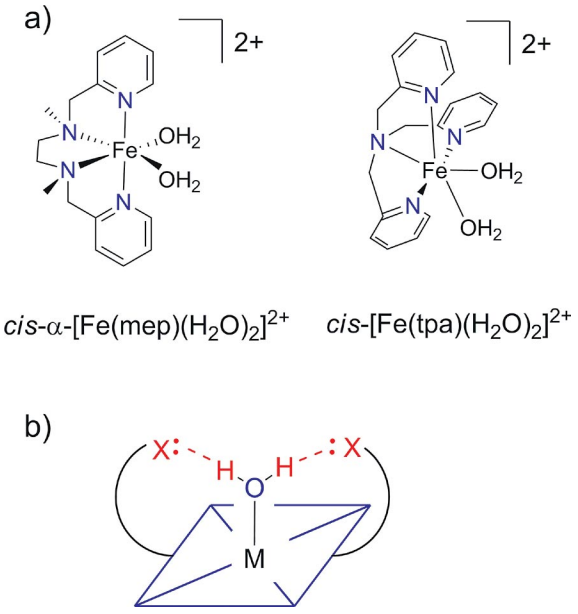

Figure 1. (a) Iron-based OER catalysts investigated by Costas and co-workers.[4] (b) Schematic representation of hydrogen-bond acceptors in the second coordination sphere (denoted in red) of a metal–aquo complex.

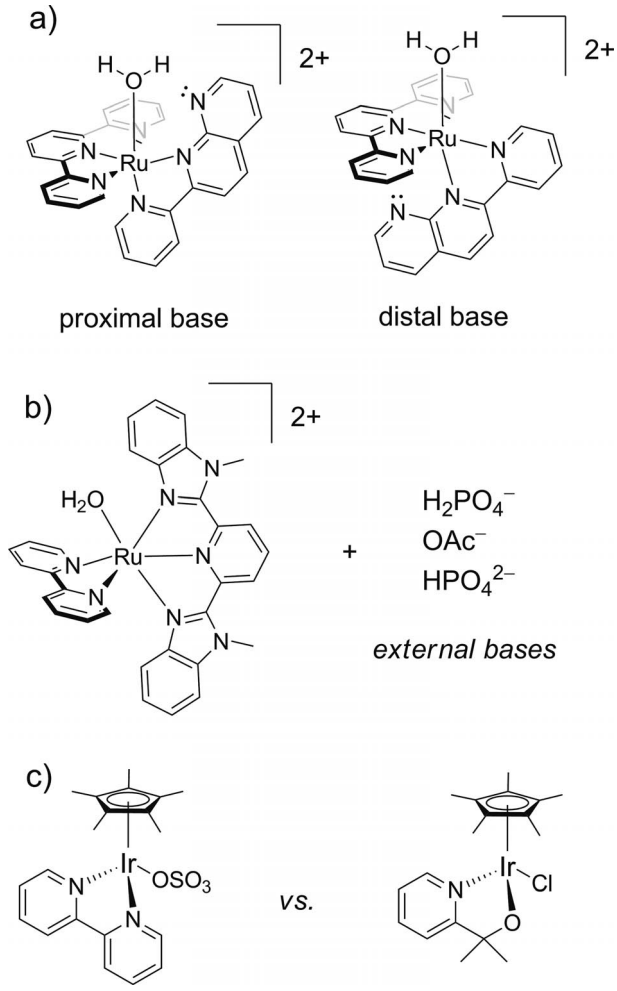

Figure 2. Water-oxidation catalysts previously investigated for base-assisted substrate deprotonation as described in the literature.[8–11]

In a report by Thummel and Fujita et al.,[8] and concurrently with a report by Yagi et al.,[9] two geometric isomers of $[Ru(tpy)(pynap)(H_2O)]^{2+}$ [tpy = 2,2′;6",2"-terpyridine; pynap = 2-(pyrid-2′-yl)-1,8-naphthyridine] in which a pyridyl substituent in the second coordination sphere was either proximal or distal from the metal center (see Figure 2, a) were tested for OER activity. In this case, the proximal base appears to be a severe detriment to the ability of the complex to catalyze the oxidation of water. However, Meyer and co-workers observed enhanced catalytic rates upon addition of external bases for single-site Ru catalysts (Figure 2, b),[10] and Crabtree and co-workers found that trading a pyridine ligand for an alkoxide functionality in [IrCp*]-based (Cp* = pentamethylcyclopentadienyl) complexes results in a nearly 100-fold rate increase for water oxidation at an elevated pH. It is suggested that the internal alkoxide base deprotonates substrate water, thereby allowing for an enhanced turnover frequency (Figure 2, c).[11]

One of the reasons oxidizing water is so challenging from a synthetic standpoint is that two substrates must come together for an O–O bond to be formed during the catalytic cycle. Privalov, Llobet, Sun, and co-workers recently described an extraordinarily fast homogeneous catalytic system in which π-type interactions between adjacent Ru^{V}=O complexes led to O–O bond formation through a radical coupling pathway.[12] An alternative bond-forming mechanism employs water nucleophilic attack on a high-valent metal–oxo species. Cramer and co-workers recently undertook a computational study of the nucleophilic-attack mechanism of oxidation catalysis in the Fe^{III}(TAML) (TAML = tetraamido macrocyclic ligand) family of complexes.[13] Importantly, the authors conclude that for this system, the aqueous solvent shell serves to relay protons away from the reacting species. Given that proton-coupled electron-transfer (PCET) processes have been shown to be instrumental in driving the OER,[14] we set out to study the effects of integrating heteroatoms that can accept transient hydrogen bonds into the second coordination sphere of a known Fe-based OER catalytic platform.[4] Specifically, the incorporation of heteroatoms that might be capable of facilitating intramolecular proton transfer has been pursued in an attempt to enhance catalytic rates and/or reduce overpotentials by reducing barriers that result from high-energy intermediates.

The function and activity of molecular water-oxidation catalysts is acutely sensitive to many structural and electronic factors. Herein, we restrict our study to the effects of proton-accepting groups in close proximity to an iron center toward water-oxidation catalysis, although we recognize that more distal groups might play important roles as well. This structural theme has also been explored to some extent for Mn–aquo and Fe–hydroperoxo complexes, which are intermediates along proposed OER catalytic cycles.[15] It is

established that the *cis*-$[FeN_4L_2]^{2+}$ complexes are active toward water oxidation, so we have attempted to preserve the essential structural theme while incorporating pendant bases into the second coordination sphere.[4] Herein, we report the syntheses, structures, electrochemistry, and catalytic data for a family of new Fe^{II} complexes with heteroatoms in the second coordination sphere.

Results

Synthesis and Structural Characterization

The new reported tetradentate ligands **L**^{1}–**L**^{7} were prepared by straightforward synthetic routes analogous to the syntheses of previously reported complexes that lack the additional heteroatoms. All of the intermediates and final ligands were characterized by ^{1}H NMR spectroscopy, and the details of the syntheses and spectroscopic characterization are presented in the Supporting Information. After isolating ligands **L**^{1}–**L**^{7}, each was added to an equivalent of $FeCl_2$ to generate the corresponding Fe^{II} complexes. The desired *cis* six-coordinate complexes were isolated for ligands **L**^{1}, **L**^{2}, **L**^{3}, **L**^{4}, and **L**^{5} to give complexes [Fe(**L**^{1})Cl_2], [Fe(**L**^{2})Cl_2], [Fe(**L**^{3})Cl_2], [Fe(**L**^{4})Cl_2], and [Fe(**L**^{5})Cl_2], respectively. Coordinatively unsaturated complexes [Fe_2(**L**^{6})Cl_4] and [Fe(κ^3-**L**^{7})Cl_2] were also prepared by mixing stoichiometric amounts of the appropriate ligands and $FeCl_2$. All complexes were characterized by ^{1}H NMR spectroscopy, and purities were determined by elemental analysis. In addition to the chlorido complexes described above, analogous complexes that lack the chloride anions were prepared to preclude competitive binding of chloride in place of water during catalysis. Anion exchange to the more weakly coordinating triflate anion (OTf) was achieved through reaction with two equivalents of silver triflate. The corresponding complexes are shown in Figure 3. Compounds [Fe(**L**^{1})$(CH_3CN)_2]^{2+}$, [Fe(**L**^{2})$(OTf)_2$], [Fe(**L**^{3})Cl_2], [Fe(**L**^{4})Cl_2], [Fe(**L**^{5})$(dmf)_2]^{2+}$, [Fe_2(**L**^{6})Cl_4], and [Fe(κ^3-**L**^{7})Cl_2] were characterized by single-crystal X-ray crystallography, and the structures are presented in Figure 4. Table 1 also contains selected average bond lengths for these compounds.

For complexes of Fe^{II}, ligands **L**^{1}, **L**^{4}, and **L**^{5} enforce an α-*cis* topology, which has the aromatic amines *trans* to each other.[16] In this ligand conformation, both hydrogen-bonding or proton-accepting functionalities are poised toward the labile coordination sites. The relevant intramolecular distances from the heteroatom to the labile ligand ("X"···**L**) are given in Table 1. The structure of [Fe(**L**^{1})$(CH_3CN)_2]^{2+}$ was determined by using crystals grown from acetonitrile and is consistent with the presence of a low-spin $S = 0$ Fe^{II} center with an average Fe–N bond length of 1.973(1) Å. Diffusion of diethyl ether into a concentrated solution of [Fe(**L**^{2})$(OTf)_2$] in dichloromethane also provided single crystals suitable for X-ray crystal analysis. In this case, the triflate anions are coordinated, which results in a high-spin complex as demonstrated by significantly longer Fe–N (ca. 2.2 Å) bond lengths than for [Fe(**L**^{1})$(CH_3CN)_2]^{2+}$. In contrast to the *cis*-α ligand topology observed for [Fe(**L**^{1})$(CH_3CN)_2]^{2+}$, [Fe(**L**^{4})Cl_2], and [Fe(**L**^{5})$(dmf)_2]^{2+}$, the crystal structures of [Fe(**L**^{3})Cl_2] and [Fe(**L**^{3})$(OTf)_2$] (Figure 4 and Figure S11 in the Supporting Information) indicate that this tetradentate ligand coordinates the metal center in a *cis*-β fashion with the pyridine functionalities *cis* to each other.

All of the six-coordinate complexes were characterized by ^{1}H NMR spectroscopy. The CD_3CN spectra for [Fe(**L**^{1})$]^{2+}$ and [Fe(**L**^{2})$]^{2+}$ indicate diamagnetic Fe^{II} com-

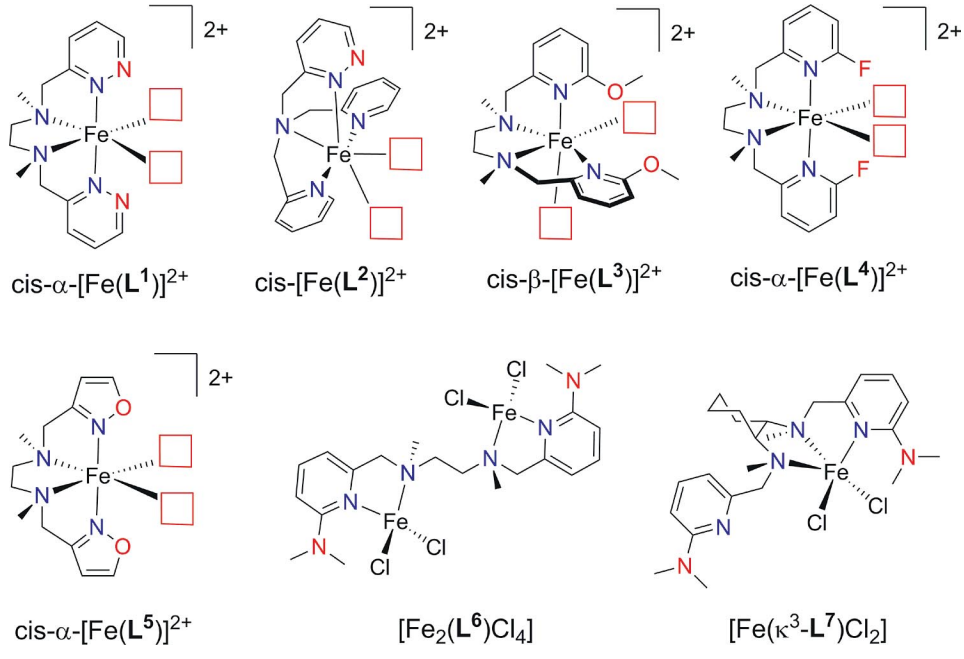

Figure 3. Schematic representations of the prepared Fe^{II} complexes. Red boxes correspond to labile coordination sites that are occupied either by solvent molecules or anionic ligands.

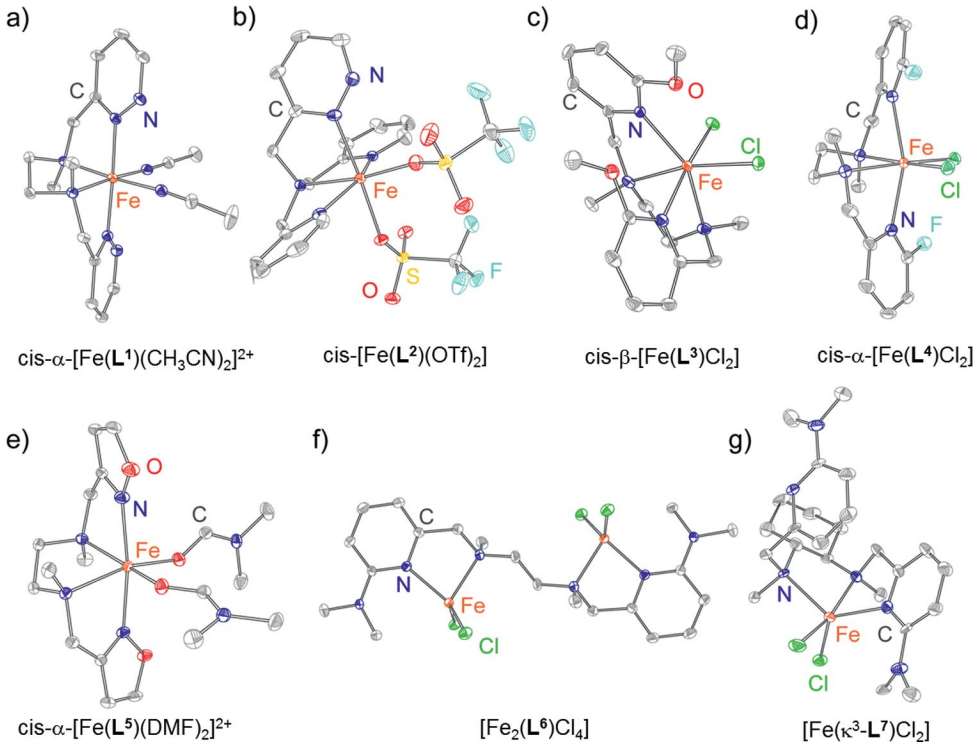

Figure 4. Thermal ellipsoid plots of the structures of the Fe^{II} complexes in (a) $[Fe(\mathbf{L^1})(CH_3CN)_2]^{2+}$, (b) $[Fe(\mathbf{L^2})(OTf)_2]$, (c) $[Fe(\mathbf{L^3})Cl_2]$, (d) $[Fe(\mathbf{L^4})Cl_2]$, (e) $[Fe(\mathbf{L^5})(dmf)_2]^{2+}$, (f) $[Fe_2(\mathbf{L^6})Cl_4]$, and (g) $[Fe(\mathbf{L^7})Cl_2]$ with thermal ellipsoids rendered at 40% probability. Orange, blue, gray, red, green, cyan, and yellow ellipsoids correspond to iron, nitrogen, carbon, oxygen, chlorine, fluorine, and sulfur atoms, respectively. Hydrogen atoms, uncoordinated counterions, and solvents have been omitted for clarity.

Table 1. Selected average bond lengths [Å] for Fe^{II}complexes with ligands $\mathbf{L^1}$–$\mathbf{L^7}$.

	$[Fe(\mathbf{L^1})(CH_3CN)_2]^{2+}$	$[Fe(\mathbf{L^2})(OTf)_2]$	$[Fe(\mathbf{L^3})Cl_2]$	$[Fe(\mathbf{L^4})Cl_2]$	$[Fe(\mathbf{L^5})(dmf)_2]^{2+}$	$[Fe_2(\mathbf{L^6})Cl_4]$	$[Fe(\mathbf{L^7})Cl_2]$
$Fe–N_{amine}$	2.0257(13)	2.2163(16)[a]	2.2989(10)	2.269(3)	2.2301(12)	2.1614(13)[a]	2.246(2)
$Fe–N_{imine}$	1.9558(13)	2.1629(16)	2.2420(9)	2.301(2)	2.1737(13)	2.1123(13)[a]	2.204(2)[a]
$Fe–\mathbf{L}_{cis}$	1.9400(14)	2.0950(14)	2.4410(3)	2.3963(9)	2.0632(11)	2.2548(4)	2.3504(8)
"X"···$\mathbf{L}_{cis}$	2.97	3.28	3.41	3.24	3.42	–	3.48

[a] Reported value is from a single measured bond length.

plexes, and the resonances could be assigned in a manner consistent with the solid-state structures. However, solutions of $[Fe(\mathbf{L^1})]^{2+}$ and $[Fe(\mathbf{L^2})]^{2+}$ in neutral D_2O contain broad, paramagnetically shifted resonances (see Figures S8 and S9 in the Supporting Information). Evans' method measurements confirm that the complexes are high-spin (S = 2) when dissolved in pH 7 water. The number of resonances and their integrated values are consistent with the structures observed in the solid-state and acetonitrile solution, and the lack of free-ligand resonances implies that the complexes $[Fe(\mathbf{L^1})]^{2+}$ and $[Fe(\mathbf{L^2})]^{2+}$ are stable in pH 7 aqueous solution. Consistent with observations from Browne and co-workers, however, ^{1}H NMR spectra of $[Fe(\mathbf{L^1})]^{2+}$ and $[Fe(\mathbf{L^2})]^{2+}$ recorded in 0.2 M triflic [D]acid in D_2O (pH = 0.7) only contain resonances that correspond to the free ligands, thus indicating that the complexes become fully dissociated under highly acidic aqueous conditions (Figure S10 in the Supporting Information).[17]

^{1}H NMR spectra for complexes $[Fe(\mathbf{L^3})]^{2+}$, $[Fe(\mathbf{L^4})]^{2+}$, and $[Fe(\mathbf{L^5})]^{2+}$ were also recorded. Unlike $[Fe(\mathbf{L^1})]^{2+}$ and $[Fe(\mathbf{L^2})]^{2+}$, these complexes are high spin in both acetonitrile and pH 7 D_2O. The N_2-sparged D_2O spectra all contain broad, paramagnetically shifted resonances, and the magnetic susceptibility measurements are all consistent with an S = 2 spin state for the Fe^{II} complexes. Taking the paramagnetic resonances alone, the spectra are all consistent with the structures determined from X-ray crystallography. However, observation of resonances for the free ligand in addition to the resonances for the paramagnetic complexes suggests that some ligand dissociation occurs when complexes $[Fe(\mathbf{L^3})]^{2+}$, $[Fe(\mathbf{L^4})]^{2+}$, and $[Fe(\mathbf{L^5})]^{2+}$ are dissolved in pH 7 water. The relative integration values for the free ligand do not significantly change over the course of three days, but the extent of dissociation was not investigated further. The greatest extent of dissociation was observed for approximately 10 mM complexes of $\mathbf{L^5}$, for which

the relative integration of the high-spin $[Fe(N_4)]^{2+}$ fragment to free-ligand resonances suggest a 3:1 molar ratio of complex to free ligand in solution. However, these estimates are based on integration and might be unreliable since one species is paramagnetic and one is diamagnetic.

Electrochemistry in Acetonitrile

The redox properties of the complexes were investigated in both acetonitrile and aqueous solution by cyclic voltammetry, with all voltammograms collected at a scan rate of 100 mV s^{-1} unless otherwise specified. In acetonitrile, pyridazine-containing complexes $[Fe(\mathbf{L^1})]^{2+}$ and $[Fe(\mathbf{L^2})]^{2+}$ exhibit fully reversible, one-electron redox waves at +0.77 V versus $Cp_2Fe^{+/0}$ (Cp = cyclopentadienyl) that correspond to the metal-centered $[Fe(N_4)(CH_3CN)_2]^{3+/2+}$ redox couples. Upon addition of 2.6 M water to a 1 mM solution of $[Fe(\mathbf{L^1})]^{2+}$ in acetonitrile, the reversible wave was replaced by a broad, irreversible wave at $E_{p/2}$ = +0.55 V versus $Cp_2Fe^{+/0}$ (Figure 5).

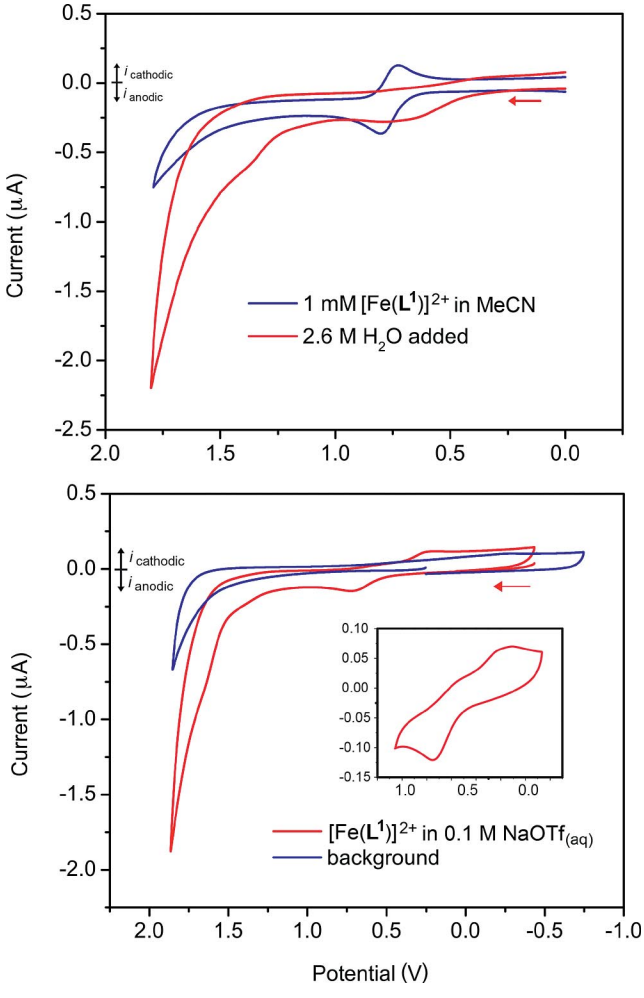

Figure 5. Top: Cyclic voltammograms of compound $[Fe(\mathbf{L^1})]^{2+}$ in acetonitrile without added water (blue trace) and with 2.6 M water (red trace), with potentials reported versus the $Cp_2Fe^{+/0}$ couple. Bottom: Cyclic voltammograms of compound $[Fe(\mathbf{L^1})]^{2+}$ in 0.1 M aqueous sodium triflate (red trace) and the corresponding background without $[Fe(\mathbf{L^1})]^{2+}$ (blue trace), with the potentials reported versus NHE. Inset: CV of the quasi-reversible Fe^{III}/Fe^{II} region.

Complexes $[Fe(\mathbf{L^3})]^{2+}$ and $[Fe(\mathbf{L^5})]^{2+}$ exhibit redox couples at higher positive potentials in acetonitrile than measured for $[Fe(\mathbf{L^1})]^{2+}$ and $[Fe(\mathbf{L^2})]^{2+}$, and the voltammograms display large peak-to-peak separations for the anodic and cathodic waves (ΔE_p = 0.26 and 0.28 V, respectively), which suggests an electrochemically irreversible process. The cyclic voltammogram for complex $[Fe(\mathbf{L^4})]^{2+}$ contains a single redox wave at $E_{p/2}$ = +1.10 V in the anodic scan, and this wave is chemically irreversible, as there is no peak observed in the return scan. The cyclic voltammetry data for all compounds in acetonitrile are presented in the Supporting Information and Table 2.

Table 2. Cyclic voltammetry data for Fe^{II} complexes with ligands $\mathbf{L^1}$–$\mathbf{L^5}$ in acetonitrile.[a]

	E_{pa} [V][b]	E_{pc} [V][c]	$E_{1/2}$ [V]
$[Fe(\mathbf{L^1})]^{2+}$	0.80	0.73	0.77
$[Fe(\mathbf{L^2})]^{2+}$	0.81	0.73	0.77
$[Fe(\mathbf{L^3})]^{2+}$	0.97	0.71	0.84[d]
$[Fe(\mathbf{L^4})]^{2+}$	1.10	0.96	1.03[d]
$[Fe(\mathbf{L^5})]^{2+}$	1.17	0.89	1.03[d]

[a] For the $Fe^{III/II}$ redox couple. All potentials are reported relative to the $Cp_2Fe^{+/0}$ redox couple. [b] Anodic peak potential. [c] Cathodic peak potential. [d] Quasi-reversible redox couple.

Electrochemistry in Water

Anodic scans with solutions of $[Fe(\mathbf{L^1})]^{2+}$ and $[Fe(\mathbf{L^2})]^{2+}$ in aqueous 0.1 M sodium triflate (pH 7.4) contain redox events at +0.73 and +0.70 V versus NHE, respectively. As the potential of the anodic scan approaches the edge of the solvent window, a slight shoulder is observed at approximately +1.6 V versus NHE for both complexes. Return cathodic scans indicate the presence of peaks at potentials of +0.24 and +0.11 V, respectively. Irreversible, one-electron oxidation waves at +0.76 and +1.30 V versus NHE are present in the voltammogram of $[Fe(\mathbf{L^3})]^{2+}$ in water. For $[Fe(\mathbf{L^4})]^{2+}$, waves at +0.87 and +1.43 V are present in the anodic scans; however, the broadness of these peaks suggests different electrochemical processes than for the waves for complexes that contain ligands $\mathbf{L^1}$–$\mathbf{L^3}$. Interestingly, complex $[Fe(\mathbf{L^5})]^{2+}$ displays a quasi-reversible redox couple with a large peak-to-peak separation (ΔE_p = 0.39 V) at much less positive potentials ($E_{1/2}$ = +0.10 V) than the other complexes studied here. When colorless aqueous solutions of $[Fe(\mathbf{L^5})]^{2+}$ were exposed to air, the color rapidly changed to dark green, consistent with the relatively mild potential for oxidation.

Estimation of Pyridazine Substituent pK_a

The acid–base equilibrium of monopyridazine complex $[Fe(\mathbf{L^2})]^{2+}$ was investigated in acetonitrile solution by mixing with one equivalent of *p*-bromoanilinium tetrafluoro-

borate (pK_a in MeCN = 9.43). Under these conditions, the conjugate acid and base forms of both molecules undergo rapid exchange, and the weighted average of the chemical shifts was used to determine the ratio of acid-to-base forms of each species.[18] From this ratio the acetonitrile pK_a of the protonated ancillary N atom was determined to be 8.0. By using water/acetonitrile pK_a correlations previously reported by Leito and co-workers, we estimated the corresponding pK_a value in water as approximately 2.[19]

Addition of Chemical Oxidants

Upon addition of ceric ammonium nitrate (CAN; 6 equiv.), yellow-orange aqueous solutions of complexes $[Fe(\mathbf{L^1})]^{2+}$ and $[Fe(\mathbf{L^2})]^{2+}$ developed a green color and exhibited new absorbances at 751 and 730 nm, respectively (Figure 6). Adding much larger amounts (ca. 1000 equiv.) of CAN to $[Fe(\mathbf{L^1})]^{2+}$ and $[Fe(\mathbf{L^2})]^{2+}$ caused visible gas evolution. In contrast, addition of CAN (6 equiv.) to solutions of complexes with ligands $\mathbf{L^3}$–$\mathbf{L^5}$ did not result in the appearance of a new absorption band in the visible spectrum, and the formation of gas bubbles was not observed upon mixture with excess amounts of CAN (Figure S12 in the Supporting Information).

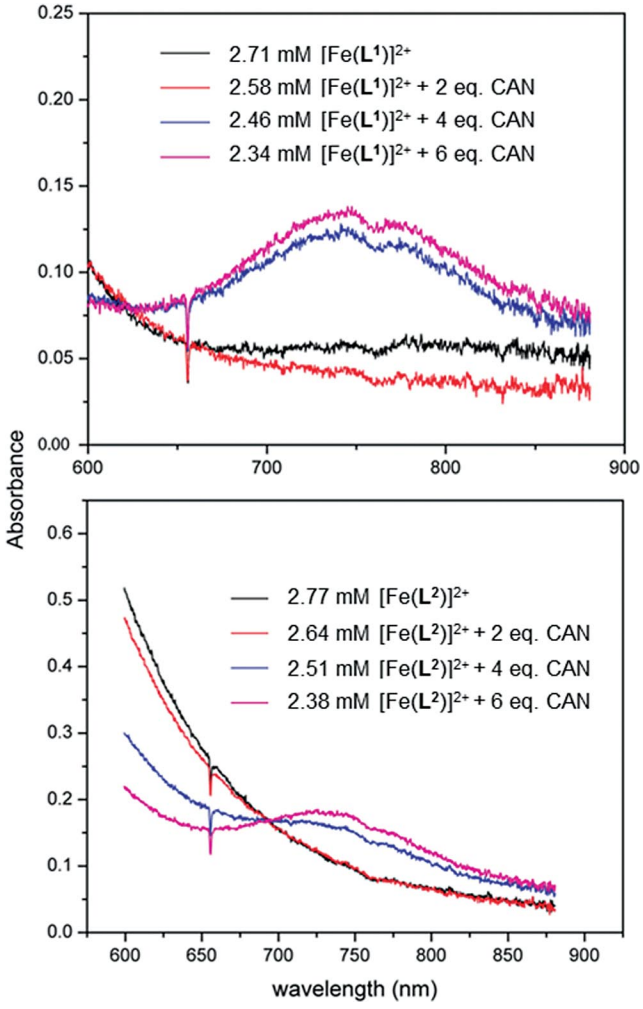

Figure 6. Visible absorption spectra of $[Fe(\mathbf{L^1})]^{2+}$ (top) and $[Fe(\mathbf{L^2})]^{2+}$ (bottom) upon addition of aliquots of CAN solution.

To measure the catalytic activity of $[Fe(\mathbf{L^1})]^{2+}$ and $[Fe(\mathbf{L^2})]^{2+}$ for the OER, a fluorescence probe was used to monitor the dioxygen partial pressure over time in the headspace of a sealed reaction vessel that contained a solution of 0.1 mM catalyst and 125 mM of a chemical oxidant prepared from pH 7 water. Qualitative evidence for OER was obtained from a gas chromatogram of the headspace, which confirmed the O_2 as the only detectable gaseous product (Figure S13 in the Supporting Information). After converting the partial pressure data to turnover numbers (TON), the initial observed turnover frequencies (TOF) were calculated by measuring the slope of the initial linear portion in plots of the TON versus time. The initial TOF for oxygen evolution reactions that employed CAN catalyzed by $[Fe(\mathbf{L^1})]^{2+}$ was determined to be 141 h^{-1}, and the catalytic activity began to level off after approximately 1 h. As shown in Figure 7 and Table 3, $[Fe(\mathbf{L^1})]^{2+}$ shows a lower initial TOF than structurally related $[Fe(mep)]^{2+}$ (mep = *N*,*N*′-dimethyl-*N*,*N*′-bis(2-pyridylmethyl)ethane-1,2-diamine) under CAN conditions, but the TON values are within one standard deviation and therefore the difference is statistically insignificant. In contrast, a slight improvement in both TOF and TON is observed for $[Fe(\mathbf{L^2})]^{2+}$ relative to the analogous $[Fe(tpa)]^{2+}$. When the reaction was repeated using oxidant and catalyst stock solutions prepared using 0.2 M HNO_3 as a diluent (pH = 0.7), the O_2 partial pressure barely increased over a period of 1 h, which corresponded to a TON of 3 (Figure S14 in the Supporting Information). As a control experiment, a solution that contained 0.1 mM $FeSO_4$ and 125 mM Ce^{IV} was monitored for OER activity. The mixture yields negligible amounts of O_2, thus demonstrating that free Fe^{II} ions do not catalyze the OER using the neutral water conditions described here (Figure S15 in the Supporting Information).

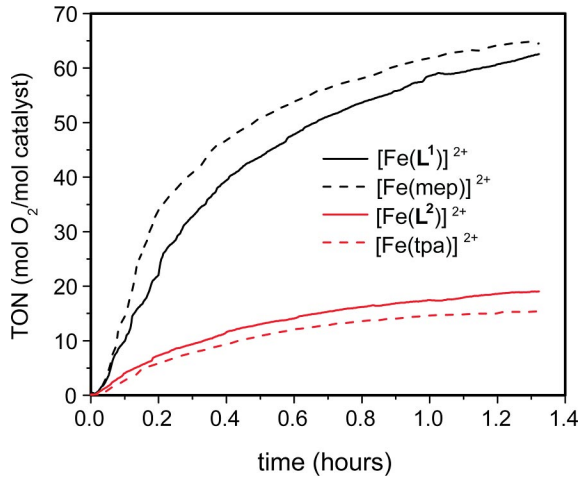

Figure 7. Turnover number (TON) versus time for structurally related complexes with (solid lines) and without (dashed lines) proton relays using Ce^{IV} as the oxidant. Catalyst and CAN solutions were prepared from pH 7 water.

Table 3. Reaction conditions and catalytic data for catalytically active complexes. All reactions were performed at 23 °C.

Catalyst	[Catalyst] [mM]	Oxidant	[Oxidant] [mM]	pH	TON[a]	TOF [h^{-1}][b]	Yield [%][c]	Ref.
$[Fe(mep)]^{2+}$	0.0125	CAN	125	–	145(5)	503	5.8	[4]
$[Fe(mep)]^{2+}$	0.1	CAN	125	0.7	72(5)	228(12)	23	this work
$[Fe(\mathbf{L^1})]^{2+}$	0.1	CAN	125	0.7	67(2)	141(12)	21	this work
$[Fe(mep)]^{2+}$	0.1	$NaIO_4$	125	4.7	42(6)	14(1)	13	this work
$[Fe(\mathbf{L^1})]^{2+}$	0.1	$NaIO_4$	125	4.7	9(1)	24(2)	2.9	this work
$[Fe(tpa)]^{2+}$	0.0125	CAN	125	–	40(4)	53	1.6	[4]
$[Fe(tpa)]^{2+}$	0.1	CAN	125	0.7	14(1)	36(3)	4.5	this work
$[Fe(\mathbf{L^2})]^{2+}$	0.1	CAN	125	0.7	20(1)	42(4)	6.4	this work

[a] TON = mol O_2/mol catalyst. [b] Initial rate. [c] The theoretical yield for each reaction is 31.3 mmol O_2 based on an initial oxidant concentration of 125 mM.

As an alternative to Ce^{IV}, sodium periodate ($NaIO_4$) may also be used as a chemical oxidant for water oxidation. $NaIO_4$ has considerably less oxidizing potential than Ce^{IV}, with a constant overpotential for water oxidation of approximately 420 mV between pH 2 and 7. For comparison, the analogous overpotential for Ce^{IV} is approximately 500 mV at pH 0.[11] The catalytic activities for $[Fe(mep)]^{2+}$ and $[Fe(\mathbf{L^1})]^{2+}$ were evaluated by using sodium periodate at pH 4.7 as described above for CAN. As shown in Table 3, the rate of dioxygen evolution using $NaIO_4$ was substantially reduced for both $[Fe(mep)]^{2+}$ and $[Fe(\mathbf{L^1})]^{2+}$ relative to the CAN reactions. This is expected given the lower oxidation potential. However, we observed small differences in the observed rate of O_2 evolution when using pyridazine-containing catalyst $[Fe(\mathbf{L^1})]^{2+}$ (24 h^{-1}) instead of $[Fe(mep)]^{2+}$ (14 h^{-1}). As indicated in the inset of Figure 8 and Table 3, although the turnover frequency at the beginning of the $[Fe(\mathbf{L^1})]^{2+}$ reaction was slightly faster than for $[Fe(mep)]^{2+}$, oxygen evolution ceased after 2 h, whereas the catalytic activity for $[Fe(mep)]^{2+}$ was maintained for approximately 10 h.

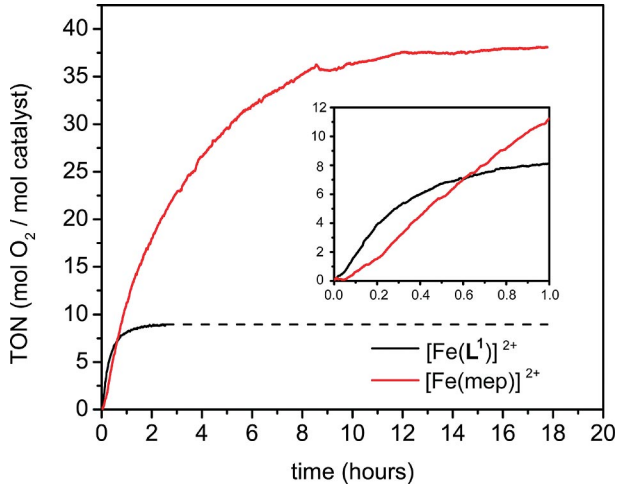

Figure 8. Turnover number (TON) versus time for $[Fe(\mathbf{L^1})]^{2+}$ and $[Fe(mep)]^{2+}$ using $NaIO_4$ as the oxidant at pH 4.7. The dashed line indicates extrapolated TON values.

Discussion

Synthesis and Structural Characterization

The desired six-coordinate *cis* complexes were obtained for ligands $\mathbf{L^1}$–$\mathbf{L^4}$ and $\mathbf{L^7}$. In noncoordinating solvents, the labile *cis*-coordination sites are occupied by anionic chlorides or triflates, but the ligands are easily displaced with solvent molecules when the complexes are dissolved in acetonitrile or water. Similar coordination behavior was expected for ligands that were functionalized with ancillary dimethylamine substituents, as simple ball-and stick models suggest that the desired Fe^{II} complex is not strongly hindered by the dimethylamines, but reactions with $\mathbf{L^5}$ gave dinuclear products. By replacing the flexible ethylenediamine bridge present in $\mathbf{L^5}$ with a more rigid cyclohexyldiamine backbone, the desired tetradentate coordination was expected to be observed.[20] However, the reaction with a racemic mixture of cyclohexyldiamine derivative $\mathbf{L^6}$ did not achieve the desired complex. Although the ligand rigidity does appear to enforce a monometallic chelation, the only isolable complex contains an isomer in which one of the pyridine groups is not coordinated to the metal center, as illustrated in Figure 4 (g). Thus, it appears that the incorporation of positioned dimethylamine groups into the tetradentate aminopyridine ligand platform described herein results in a change in coordination geometry. Specifically, the desired *cis*-α orientation in which both of the noncoordinated heteroatom groups were positioned near the labile ligands does not appear to be attainable through this approach.

Electrochemistry in Acetonitrile

In dry acetonitrile, the only electrochemical event observed for $[Fe(\mathbf{L^1})(CH_3CN)_2]^{2+}$ was a one-electron metal-centered redox couple. After water was added, this couple was replaced with a broad, irreversible wave at slightly less positive potentials. This new wave was tentatively assigned to the formation of $[Fe^{III}(\mathbf{L^1})(H_2O)(OH)]^{2+}$ species in the basis of a similar observation for $[Fe^{II}(N_4Py)(CH_3CN)]^{2+}$ [N_4Py = *N*,*N*-bis(2-pyridylmethyl)-*N*-bis(2-pyridyl)methylamine].[21] Upon scanning to more positive potentials, a broad irreversible wave of larger amplitude appeared at +1.3 V versus $Cp_2Fe^{+/0}$. Que and co-workers generated the $[Fe(N_4Py)(O)]^{2+}$ complex by using bulk electrolysis in wet acetonitrile at the same potential (+1.3 V) starting from $[Fe^{III}(N_4Py)(CH_3CN)_2]^{2+}$ despite the lack of a corresponding anodic wave in the cyclic voltammogram.[21] Here, the visible absorption spectrum of an aliquot of a solution of $[Fe(\mathbf{L^1})(CH_3CN)_2]^{2+}$ after bulk electrolysis (+1.4 V versus

$Cp_2Fe^{+/0}$) in wet acetonitrile did not contain a peak at approximately 750 nm and is therefore inconsistent with the formation of $[Fe^{IV}(\mathbf{L^1})O]^{2+}$. This result likely reflects the high kinetic barrier to Fe^{IV}=O formation using electrochemical methods for this family of complexes.

Electrochemistry in Water

The cyclic voltammograms of $[Fe(\mathbf{L^1})]^{2+}$ and $[Fe(\mathbf{L^2})]^{2+}$ recorded in aqueous solution do not contain features that are readily interpretable. Irreversible, low-amplitude waves at mild potentials are most consistent with metal-centered redox events, and the lack of S-shaped waves at higher applied potentials suggests that the OER catalytic activity observed with chemical oxidants might not be measurable using cyclic voltammetry. Ultimately, we aim to characterize the catalytic activity of synthetic water oxidation catalysts by using electrochemical techniques, but the catalytic rates observed for this family of complexes are too slow for determination of catalytic rates by cyclic voltammetry (see below).[4]

Catalytic Oxidation of Water

The addition of a slight stoichiometric excess amount of CAN to solutions of $[Fe(\mathbf{L^1})]^{2+}$ and $[Fe(\mathbf{L^2})]^{2+}$ results in the appearance of a new peak in the visible absorption spectrum at 749 and 731 nm, respectively. None of the other complexes described herein exhibited analogous behavior. On the basis of similar observations made by Costas and co-workers for *cis*-$[Fe(N_4)X_2]$ complexes, these absorbance bands are consistent with the formation of $[Fe^{IV}(N_4)O]^{2+}$ species, which are necessary participants in the OER catalytic cycle. A twofold excess amount of CAN is required to observe the Fe^{IV} species, which suggests that accessing the high-valent oxidation state requires additional CAN to push the equilibrium redox reaction to completion. These results and observations suggest that the pyridazine substituents present in $\mathbf{L^1}$ and $\mathbf{L^2}$ support ferryl ions, but that ligand fields imparted by $\mathbf{L^3}$–$\mathbf{L^5}$ are not sufficient to stabilize the high-valent Fe center necessary for OER catalysis.

By using solutions of CAN prepared from pH 7 water, the catalytic activity for the OER is similar for structurally related complexes with and without heteroatoms in the second coordination sphere. The highly acidic medium that is generated by dissolving CAN in water might defeat the purpose of incorporating the heteroatoms adjacent to the metal center. Considering that the pH of the 125 mM CAN-containing solutions used here was measured at 0.7, the ancillary nitrogen atoms are likely to be protonated under the conditions used for the chemical oxidation experiments, thus suggesting that the minor observed differences in catalyst lifetime and rate might be electronic in origin and are not influenced by the proton-accepting ability of the ancillary nitrogen atoms. More importantly, the ^{1}H NMR spectroscopic data indicates that ligand dissociation occurs at pH 0.7. Taken together with the lack of OER observed with free Fe^{2+}, these results implicate $[Fe(\mathbf{L^1})]^{2+}$ and $[Fe(\mathbf{L^2})]^{2+}$ as active homogeneous catalysts and point toward acid-driven ligand dissociation as the likely reason for eventual catalyst death. Furthermore, although we did not investigate the possible presence of nanoparticles for the OER reactions, Costas and co-workers have followed the OER reaction using analogous catalysts by dynamic light-scattering techniques and found no evidence for nanoparticle formation upon reaction with CAN.[4] To avoid protonation of the pyridazine heteroatoms, OER studies were also performed at higher solution pH using sodium periodate as a chemical oxidant with complex $[Fe(\mathbf{L^1})]^{2+}$. The analogous studies with complex $[Fe(\mathbf{L^2})]^{2+}$ and $[Fe(tpa)]^{2+}$ did not produce measureable dioxygen, and therefore will not be discussed here. In comparing $[Fe(\mathbf{L^1})]^{2+}$ to $[Fe(mep)]^{2+}$, a significant reduction in catalyst lifetime is evident from the plot shown in Figure 8. The periodate ion is capable of participating in fast O-atom exchange with water.[22] This propensity for periodate O atoms to participate in exchange reactions might lead to the more rapid deactivation of the complex $[Fe(\mathbf{L^1})]^{2+}$ due to oxidation of the bare pyridazine N atom, which is absent in $[Fe(mep)]^{2+}$.

Conclusion

New tetradentate ligands that feature proton relays and the corresponding Fe^{II} complexes have been synthesized. In an attempt to enhance catalysis for water oxidation, pendant heteroatoms were incorporated into known catalytic platforms with the intended purpose of facilitating the shuttling of protons from the substrate to the bulk solution. In the case of $\mathbf{L^6}$ and $\mathbf{L^7}$, the resulting Fe^{II} complexes had a substantial and undesirable change in coordination mode relative to the analogous parent complex that lacked the additional heteroatoms. Ancillary heteroatoms with a lower steric footprint were successfully incorporated into ligands $\mathbf{L^1}$–$\mathbf{L^5}$, but the catalytically necessary Fe^{IV}=O species for complexes with $\mathbf{L^3}$, $\mathbf{L^4}$, and $\mathbf{L^5}$ did not appear to be accessible on the basis of absorption spectra recorded in the presence of CAN. However, the pyridazine-containing complexes $[Fe(\mathbf{L^1})]^{2+}$ and $[Fe(\mathbf{L^2})]^{2+}$ display OER catalytic activity similar to their structurally related analogues that do not contain ancillary proton relays. By adjusting the pH of the solvent medium to allow protons that originate from substrate water to interact with the pendant bases, a slight improvement was observed in the initial turnover frequency for catalyst $[Fe(\mathbf{L^1})]^{2+}$ relative to the structurally analogous $[Fe(mep)]^{2+}$. However, rapid deactivation of the $[Fe(\mathbf{L^1})]^{2+}$ catalyst was observed, possibly due to the oxidation of the ligand that resulted from the O-atom lability imparted by the periodate and the additional incorporated nitrogen atoms, which are capable of acting as O-atom acceptors. Looking ahead, the incorporation of intramolecular hydrogen-bonding functionalities might be worth considering for the design of new homogeneous water-oxidation catalysts. In addition to selecting ligand platforms capable of sup-

porting the reactive metal–oxo species necessary for catalysis, the careful choice of operating solution conditions and compatible pendant bases could afford OER catalysts with higher turnover frequencies and/or lower overpotentials.

Experimental Section

Materials and Methods: All chemicals were purchased from commercial sources and used without further purification unless otherwise noted. Solvents were sparged with N_2 for 45 min and passed through a column of alumina prior to use.

***cis*-α-[Fe(L^1)Cl$_2$]:** Under an atmosphere of dinitrogen, a solution of **L^1** (0.288 g, 1.16 mmol) in acetonitrile was added to a stirred slurry of $FeCl_2$ (0.147 g, 1.16 mmol) in acetonitrile (1 mL), thus causing a brick red solid to precipitate. After stirring for 2 h, the solid was isolated by filtration, washed with acetonitrile (2 × 2 mL) and diethyl ether (3 × 2 mL), and dried under dinitrogen to afford the final product (0.272 g, 0.725 mmol, 63% yield). Single crystals suitable for X-ray analysis were grown by diffusion of diethyl ether vapor into a dilute solution of [Fe(**L^1**)Cl$_2$] in dichloromethane. ^{1}H NMR (300 MHz, D_2O, 25 °C): δ = 172.28 (br., 1 H), 93.17 (br., 1 H), 74.72 (br., 3 H, –C*H*$_3$), 59.84 (br., 1 H), 41.36 (br., 1 H), 28.44 (br., 1 H), –17.35 (br., 1 H) ppm. $C_{14}H_{20}Cl_2FeN_6$ (399.11): calcd. C 42.13, H 5.05, N 21.06; found C 41.62, H 5.01, N 20.77.

***cis*-α-[Fe(L^2)(CH$_3$CN)$_2$](OTf)$_2$:** Under an atmosphere of dinitrogen, a solution of silver triflate (0.143 g, 0.556 mmol) in acetonitrile (5 mL) was added to a stirred slurry of [Fe(**L^1**)Cl$_2$] (0.104 g, 0.278 mmol) in acetonitrile (2 mL). After stirring the mixture for 1 h, the mixture was filtered to remove AgCl, and the solvent was removed from the filtrate. The resulting dark red residue was triturated in diethyl ether, thus causing a red solid to form. The solid was isolated by filtration, washed with diethyl ether (3 × 2 mL), and dried under dinitrogen to afford the final product (0.177 g, 0.259 mmol, 93% yield). Single crystals suitable for X-ray analysis were grown by diffusing diethyl ether vapor into a concentrated solution of **8** in acetonitrile. ^{1}H NMR (300 MHz, CD_3CN, 25 °C): δ = 9.46 (s, 2 H, pdz-*H*), 8.12 (d, 2 H, pdz-*H*), 7.79 (t, 2 H, pdz-*H*), 5.28 [d, 2 H, pdz-C*H*$_2$ (*exo*)], 4.52 [d, 2 H, pdz-C*H*$_2$ (*endo*)], 3.14 [d, 2 H, en-C*H*$_2$ (*exo*)], 2.79 (s, 6 H, –C*H*$_3$), 2.39 [d, 2 H, en-C*H*$_2$ (*endo*)], 1.96 (s, 6 H, Fe–NCC*H*$_3$) ppm. The ^{1}H NMR spectrum in D_2O matched that of *cis*-α-[Fe(**L^1**)Cl$_2$]. $C_{20}H_{26}F_6FeN_8O_6S_2$ (708.43): calcd. C 33.91, H 3.70, N 15.82; found C 34.03, H 3.72, N 15.78. μ_{eff} (D_2O) = 5.5 μ_B.

[Fe(L^2)Cl$_2$]: Under an atmosphere of dinitrogen, a solution of **L^2** (0.146 g, 0.496 mmol) in acetonitrile (5 mL) was added to a stirred slurry of $FeCl_2$ (0.063 g, 0.45 mmol) in acetonitrile (2 mL). A dark red precipitate formed immediately. After 5 min, diethyl ether (3 mL) was added to induce further precipitation. The solid was isolated by filtration, washed with acetonitrile (2 × 2 mL) and diethyl ether (3 × 2 mL), and dried under dinitrogen to afford the final product (0.125 g, 0.299 mmol, 60% yield). $C_{17}H_{17}Cl_2FeN_5$ (418.11): calcd. C 48.84, H 4.10, N 16.75; found C 49.11, H 4.10, N 16.93.

[Fe(L^2)(OTf)$_2$]: Under an atmosphere of dinitrogen, a solution of silver triflate (0.030 g, 0.11 mmol) in tetrahydrofuran (5 mL) was added to a stirred slurry of [Fe(**L^2**)Cl$_2$] (0.024 g, 0.057 mmol) in tetrahydrofuran (2 mL). After stirring for 1 h, the mixture was filtered to remove AgCl, and the solvent was removed from the filtrate. The resulting orange-yellow residue was trituted in diethyl ether, thus causing an orange-yellow solid to form. The solid was isolated by filtration, washed with diethyl ether (3 × 2 mL), and dried under dinitrogen to afford the crude product (0.022 g, 0.034 mmol, 60%). Yellow single crystals suitable for X-ray analysis were grown by diffusing diethyl ether vapor into a concentrated solution of [Fe(**L^2**)(OTf)$_2$] in dichloromethane. $C_{19.1}H_{17.2}Cl_{0.2}F_6FeN_5O_6S_2$ {[Fe(**L^2**)(OTf)$_2$]·0.1CH_2Cl_2} (653.8): calcd. C 35.09, H 2.65, N 10.71; found C 34.84, H 2.96, N 10.91. The analogous low-spin acetonitrile complex, [Fe(**L^2**)(CH$_3$CN)$_2$](OTf)$_2$, was obtained by recrystallization of [Fe(**L^2**)(OTf)$_2$] from acetonitrile. ^{1}H NMR (300 MHz, CD_3CN, 25 °C): δ = 9.42 (br. s, 2 H, Py-*H*), 9.14 (d, 1 H, pdz-*H*), 7.78 (d, 1 H, pdz-*H*), 7.71 (m, 6 H, Py-*H*), 7.49 (m, 1 H, pdz-*H*), 5.21 (s, 2 H, pdz-C*H*$_2$), 5.15 (s, 4 H, Py-C*H*$_2$) ppm. ^{1}H NMR (300 MHz, D_2O, 25 °C): δ = 145.75 (2 H), 91.16 (2 H), 55.71 (2 H), 53.60 (1 H), 50.24 (2 H), 46.59 (2 H), 33.67 (1 H), 31.05 (1 H), 26.31 (2 H), 20.42 (2 H) ppm. μ_{eff} (D_2O) = 5.3 μ_B.

***cis*-β-[Fe(L^3)Cl$_2$]:** Under an atmosphere of dinitrogen, a solution of **L^3** (0.210 g, 0.635 mmol) in acetonitrile (5 mL) was added to a stirred slurry of $FeCl_2$ (0.077 g, 0.60 mmol) in acetonitrile. After 2 h, the resulting yellow-orange solution was filtered and concentrated under vacuum. Addition of diethyl ether (15 mL) caused a yellow solid to precipitate. The solid was isolated by filtration, washed with diethyl ether (3 × 2 mL), and dried under dinitrogen to afford the final product (0.230 g, 0.503 mmol, 79% yield). Single crystals suitable for X-ray analysis were grown by diffusing diethyl ether vapor into a concentrated solution of [Fe(**L^3**)Cl$_2$] in dichloromethane. $C_{20}H_{29}Cl_2FeN_5O_2$ (498.23): calcd. C 48.21, H 5.87, N 14.06; found C 47.94, H 5.92, N 13.76.

***cis*-β-[Fe(L^3)(OTf)$_2$]:** Under an atmosphere of dinitrogen, a solution of silver triflate (0.132 g, 0.525 mmol) in acetonitrile (5 mL) was added to a stirred slurry of [Fe(**L^3**)Cl$_2$] (0.117 g, 0.256 mmol) in acetonitrile (3 mL). After stirring for 1 h, the mixture was filtered to remove AgCl, and the solvent was removed from the filtrate. The resulting pale yellow solid was washed with diethyl ether (10 mL). The solid was isolated by filtration, washed with diethyl ether (3 × 2 mL), and dried under dinitrogen to afford the final product (0.121 g, 0.173 mmol, 68% yield). ^{1}H NMR (300 MHz, D_2O, 25 °C): δ = 195.12 (br., 2 H), 99.06 (br., 2 H), 82.40 (br., 2 H), 59.86 (br., 3 H), 37.72 (br., 2 H), 32.98 (br., 4 H), 20.87 (br., 2 H), –1.38 (br., 2 H), –8.35 (br., 6 H) ppm. $C_{20.5}H_{26.75}F_6FeN_{4.25}O_8S_2$ {[Fe(**L^7**)(OTf)$_2$]·0.25CH_3CN} (694.7): calcd. C 35.44, H 3.88, N 8.57; found C 35.04, H 3.86, N 8.93.

***cis*-α-[Fe(L^4)Cl$_2$]:** Under an atmosphere of dinitrogen, a solution of **L^4** (0.527 g, 1.72 mmol) in acetonitrile (5 mL) was added to a stirred slurry of $FeCl_2$ (0.218 g, 1.72 mmol) in acetonitrile. After 2 h, the resulting yellow solid was isolated by filtration, washed with diethyl ether (3 × 2 mL), and dried under dinitrogen to afford the final product (0.488 g, 1.12 mmol, 65% yield). Single crystals suitable for X-ray analysis were grown by diffusing diethyl ether vapor into a concentrated solution of [Fe(**L^4**)Cl$_2$] in dichloromethane. $C_{18}H_{20}Cl_2F_2FeN_4$ (457.13): calcd. C 44.37, H 4.65, N 12.94; found C 44.14, H 4.68, N 12.74.

***cis*-α-[Fe(L^4)(OTf)$_2$]:** Under an atmosphere of dinitrogen, a solution of silver triflate (0.370 g, 1.44 mmol) in acetonitrile (5 mL) was added to a stirred slurry of [Fe(**L^4**)Cl$_2$] (0.311 g, 0.719 mmol) in acetonitrile (3 mL). After stirring for 1 h, the mixture was filtered to remove AgCl, and the solvent was removed from the filtrate. The resulting white solid was washed with diethyl ether (10 mL). The solid was isolated by filtration, washed with diethyl ether (3 × 2 mL), and dried under dinitrogen to afford the final product (0.376 g, 0.569 mmol, 79% yield). ^{1}H NMR (300 MHz, D_2O, 25 °C): δ = 188.21 (br., 1 H), 101.19 (br., 1 H), 82.62 (br., 1 H), 55.71 (br., 1 H), 39.25 (br., 3 H, –C*H*$_3$), 32.19 (br., 1 H), 21.12 (br.,

1 H), –1.18 (br., 1 H) ppm. $C_{18}H_{20}F_8FeN_4O_6S_2$ (660.33): calcd. C 32.74, H 3.05, N 8.48; found C 32.56, H 2.95, N 8.41. μ_{eff} (D_2O) = 5.3 μ_B.

***cis*-α-[Fe(L^5)Cl$_2$]:** Under an atmosphere of dinitrogen, a solution of **L^5** (0.507 g, 2.03 mmol) in acetonitrile (5 mL) was added to a stirred slurry of $FeCl_2$ (0.257 g, 2.03 mmol) in acetonitrile. After 1 h, the resulting pale yellow solid was isolated by filtration, washed with diethyl ether (3 × 2 mL), and dried under dinitrogen to afford the final product (0.640 g, 1.67 mmol, 83% yield). $C_{12}H_{18}Cl_2FeN_4O_2$ (377.05): calcd. C 38.23, H 4.81, N 14.86; found C 38.61, H 4.96, N 15.12.

***cis*-α-[Fe(L^5)(OTf)$_2$]:** Under an atmosphere of dinitrogen, a solution of silver triflate (0.432 g, 1.68 mmol) in acetonitrile (5 mL) was added to a stirred slurry of [Fe(**L^5**)Cl$_2$] (0.317 g, 0.842 mmol) in acetonitrile (3 mL). After stirring for 1 h, the mixture was filtered to remove AgCl, and the solvent was removed from the filtrate. The resulting white residue was triturated in diethyl ether (10 mL). The resulting solid was isolated by filtration, washed with diethyl ether (3 × 2 mL), and dried under dinitrogen to afford the final product (0.356 g, 0.589 mmol, 70% yield). Single crystals of *cis*-α-[Fe(**L^5**) (dmf)$_2$](OTf)$_2$ suitable for X-ray analysis were grown by diffusing diethyl ether vapor into a concentrated solution of [Fe(**L^5**)(OTf)$_2$] in *N*,*N*-dimethylformamide. ^{1}H NMR (300 MHz, D_2O, 25 °C): δ = 170.87 (br., 1 H), 100.41 (br., 1 H), 94.19 (br., 1 H), 67.82 (br., 3 H, –C*H*$_3$), 31.97 (br., 1 H), –0.14 (br., 1 H), –4.67 (br., 1 H) ppm. $C_{14}H_{18}F_6FeN_4O_8S_2$ (604.27): calcd. C 27.83, H 3.00, N 9.27; found C 27.55, H 2.82, N 8.98. μ_{eff} (D_2O) = 5.3 μ_B.

[Fe$_2$(L^6)Cl$_4$]: Under an atmosphere of dinitrogen, a solution of **L^6** (0.134 g, 0.377 mmol) was added to a stirred slurry of $FeCl_2$ (0.048 g, 0.38 mmol), thus causing a yellow solid to precipitate. After 1 h, the solid was isolated by filtration, washed with diethyl ether (3 × 2 mL), and dried under dinitrogen to afford the final product (0.056 g, 0.092 mmol, 48% yield based on $FeCl_2$). Crystals suitable for X-ray analysis were grown by diffusing diethyl ether vapor into a concentrated solution of [Fe$_2$(**L^6**)Cl$_4$] in dichloromethane. $C_{20}H_{32}Cl_4FeN_6$ (554.17): calcd. C 39.38, H 5.29, N 13.78; found C 39.41, H 5.28, N 13.78.

[κ^3-Fe(L^7)Cl$_2$]: Under an atmosphere of dinitrogen, a solution of **L^7** (0.311 g, 0.770 mmol) was added to a stirred slurry of $FeCl_2$ (0.097 g, 0.77 mmol), thus causing a cream-colored solid to precipitate. After 2 h, the solid was isolated by filtration, washed with diethyl ether (3 × 2 mL), and dried under dinitrogen to afford the final product. Crystals suitable for X-ray analysis were grown by diffusing diethyl ether vapor into a concentrated solution of [Fe(**L^7**)Cl$_2$] in dichloromethane. (0.272 g, 0.506 mmol, 66% yield). $C_{24.1}H_{38.2}Cl_{2.2}FeN_6$ {[Fe(**L^7**)Cl$_2$]·0.1CH_2Cl_2} (545.9): calcd. C 53.03, H 7.05, N 15.40; found C 52.87, H 7.08, N 15.19.

Electrochemistry: Electrochemical data were collected with a CH Instruments 600 or 1100 series computer-aided three-electrode potentiostat in acetonitrile with 0.1 M Bu_4NPF_6 in acetonitrile or 0.1 M NaOTf in water. For cyclic voltammetry, the working electrode was a glassy carbon disc and the counter electrode was either a glassy carbon rod or platinum wire. The reference electrode was either an Ag/AgCl reference electrode for aqueous measurements (purchased from CH Instruments) or a silver chloride coated silver wire as a pseudoreference electrode in acetonitrile, separated from the main compartment by a Vycor disc (1/8 in. diameter). For the aqueous measurements the $[(CN)_6Fe^{III}]^{3-}/[(CN)_6Fe^{II}]^{4-}$ redox couple (0.431 V versus NHE)[23] was measured at $E_{1/2}$ = 0.177 V using the setup described here. All potentials for aqueous cyclic voltammograms are reported versus NHE by adding 0.254 V to the measured potentials. For the measurements in acetonitrile, cobaltocenium hexafluorophosphate ($E_{1/2}$ = –1.33 V versus $Cp_2Fe^{+/0}$)[24] was used as an internal standard, and all potentials are reported versus the ferrocenium/ferrocene couple ($Cp_2Fe^{+/0}$). The potentials of irreversible electrochemical waves are reported as $E_{p/2}$ values (i.e., potential at half-current). Unless otherwise noted, all cyclic voltammograms were obtained at a scan rate of 100 mV s^{-1}.

X-ray Structure Determinations: Single crystals were coated in Paratone to facilitate manipulation. The crystals were supported on a Cryoloop and mounted on a Bruker Kappa Apex 2 CCD diffractometer under a stream of cold dinitrogen. All data collection was performed using Mo-K_α radiation and a graphite monochromator (Table 4). Initial lattice parameters were determined from reflections with $I > 2\sigma$ harvested from 36 frames; these parameters

Table 4. Crystallographic data[a] for complexes [Fe(**L^1**)(CH$_3$CN)$_2$]$^{2+}$, [Fe(**L^2**)(OTf)$_2$], [Fe(**L^3**)Cl$_2$]·CH$_3$CN, [Fe(**L^4**)Cl$_2$], [Fe(**L^5**)(dmf)$_2$]$^{2+}$, [Fe$_2$(**L^6**)Cl$_4$], and [Fe(κ^3-**L^7**)Cl$_2$].

	[Fe(**L^1**)(CH$_3$CN)$_2$]$^{2+}$	[Fe(**L^2**)(OTf)$_2$]	[Fe(**L^3**)Cl$_2$]·CH$_3$CN	[Fe(**L^4**)Cl$_2$]	[Fe(**L^5**)(dmf)$_2$]$^{2+}$	[Fe$_2$(**L^6**)Cl$_4$]	[Fe(κ^3-**L^7**)Cl$_2$]
Formula	$C_{20}H_{26}F_6FeN_8O_6S_2$	$C_{19}H_{17}F_6FeN_5O_6S_2$	$C_{20}H_{29}Cl_2FeN_5O_2$	$C_{16}H_{20}Cl_2FeN_4F_2$	$C_{20}H_{32}F_6FeN_6O_{10}S_2$	$C_{20}H_{32}Cl_4Fe_2N_6$	$C_{24}H_{38}Cl_2FeN_6$
M_r [g mol^{-1}]	708.46	645.35	498.23	433.11	750.49	610.02	537.35
Color, habit	red prism	yellow needle	yellow block	yellow block	yellow needle	yellow block	yellow block
T [K]	120(2)	120(2)	120(2)	120(2)	120(2)	120(2)	120(2)
Space group	$P2_1/c$	$P2_1/c$	$P2_1/c$	$P2/c$	$P\bar{1}$	$P2_1/c$	$P\bar{1}$
Z	4	4	4	4	2	2	2
a [Å]	13.7026(6)	17.6127(14)	9.9073(3)	15.5303(8)	7.6666(2)	7.1296(7)	7.9623(8)
b [Å]	18.0724(8)	9.6293(8)	21.6754(8)	8.3569(4)	11.6490(4)	15.0265(15)	9.8929(10)
c [Å]	12.4999(5)	15.8586(13)	12.9892(4)	15.6653(7)	17.5354(6)	13.5621(11)	18.086(2)
α [°]	90	90	90	90	94.688(2)	90	75.412(4)
β [°]	109.1120(10)	113.615(2)	123.896(2)	116.674(2)	92.3700(10)	113.902(4)	89.903(4)
γ [°]	90	90	90	90	91.0240(10)	90	69.453(4)
V [Å^3]	2924.8(2)	2464.4(3)	2315.31(13)	1816.75(15)	1559.13(9)	1328.3(2)	1285.1(2)
R_1,[b] wR_2[c] ($I > 2\sigma$)	0.0312, 0.0786	0.0349, 0.0813	0.0221, 0.0563	0.0400, 0.0961	0.0278, 0.0677	0.0251, 0.0581	0.0360, 0.1181
R_1,[b] wR_2[c] (all data)	0.0385, 0.0830	0.0510, 0.0882	0.0247, 0.0575	0.0567, 0.1031	0.0352, 0.0709	0.0323, 0.0604	0.0440, 0.1376
GOF	1.026	1.025	1.044	1.090	1.055	1.021	1.082

[a] Obtained with graphite-monochromated Mo-K_α radiation (λ = 0.71073 Å). [b] $R_1 = \Sigma||F_o| - |F_c||/\Sigma|F_o|$. [c] $wR_2 = \{\Sigma[w(F_o^2 - F_c^2)^2]/\Sigma[w(F_o^2)^2]\}^{1/2}$.

were later refined against all data. Data collection strategies were targeted for a minimum of 0.80 Å resolution with fourfold redundancy. Data were integrated and corrected for absorption effects with the Apex II software package. Structures were solved by direct methods and refined with the SHELXTL software package. Unless otherwise noted, all non-hydrogen atoms were refined anisotropically. Hydrogen atoms were added at the ideal positions and were refined using a riding model in which the displacement parameters were set at 1.2 times that of the attached carbon atom (1.5 times for methyl carbon atoms).

The pyridazine substituent in the structure of $[Fe(\mathbf{L^2})(OTf)_2]$ was disordered over all three N-donating positions. This was expected considering the non-stereospecific nature of the ligand synthesis and the structural similarity of pyridine and pyridazine. The disorder was modeled by splitting the carbon/nitrogen atomic sites adjacent to the coordinating nitrogen atom and restricting the carbon occupancy to 66.7% and the nitrogen occupancy to 33.3%.

Other Physical Measurements: ^{1}H spectra were recorded with Varian spectrometers (500 or 300 MHz) at 20 °C. All ^{1}H chemical shifts have been internally calibrated to the monoprotio impurity of the deuterated solvent. For spectra taken in deuterium oxide, the D_2O was sparged with N_2 for a minimum of 20 min prior to dissolution of the compound to prevent reaction with O_2. Magnetic susceptibility measurements were made using Evans' method.[25] Diamagnetic contributions to the susceptibility were accounted for using Pascal's constants. Elemental analysis was performed by Atlantic Microlab, Inc. (Norcross, GA).

Chemical Oxidation for O_2 Evolution: Dioxygen evolution was monitored in the headspace of reactions in 24.0 mL of EPA vials equipped with polytetrafluoroethylene (PTFE)-faced silicone rubber septum caps. The O_2 partial pressure was measured with an Ocean Optics Neofox Phase Measurement System equipped with a FOXY-R probe, temperature sensor, and a septum-puncturing accessory. The instrument was calibrated before each set of runs by using an N_2-filled flask and ambient air as 0.0 and 20.9% O_2 standards, respectively. Each vial was charged with either solid cerium(IV) ammonium nitrate (0.685 g, 1.25 mmol) or sodium *meta*-periodate (0.267 g, 1.25 mmol), then purged with N_2 until the concentration of O_2 was at a stable minimum. The oxidant was then dissolved in N_2-sparged Milli-Q water (9.0 mL; ρ = 18.2 MΩ cm^{-1}) with stirring (450 rpm). The catalytic reaction was initiated by adding an N_2-sparged 1 mM stock solution of catalyst in Milli-Q water (1.0 mL). The final concentrations of catalyst and oxidant were 0.1 and 125 mM, respectively. After the reaction was complete, the partial pressure data in the reaction vial headspace was converted to mol amounts of O_2 by using the ideal gas law, and the dissolved oxygen content was determined using Henry's law; these two values were added together to arrive at the total amount of evolved O_2.

CCDC-908874 {for $[Fe(\mathbf{L^1})(CH_3CN)_2](OTf)_2$}, -908875 {for $[Fe(\mathbf{L^2})(OTf)_2]$}, -908876 {for $[Fe(\mathbf{L^4})Cl_2]$}, -908877 {for $[Fe(\mathbf{L^3})Cl_2]$}, -908878 {for $[Fe(\mathbf{L^5})(dmf)_2](OTf)_2$}, -908879 {for $[Fe_2(\mathbf{L^6})Cl_4]$}, and -908880 {for $[Fe(\kappa^3\text{-}\mathbf{L^7})Cl_2]$} contain the supplementary crystallographic data for this paper. These data can be obtained free of charge from The Cambridge Crystallographic Data Centre via www.ccdc.cam.ac.uk/data_request/cif.

Supporting Information (see footnote on the first page of this article): Experimental details for ligand preparation, ^{1}H NMR spectra for ligands $\mathbf{L^1}$–$\mathbf{L^7}$ and complexes $[Fe(\mathbf{L^1})]^{2+}$ and $[Fe(\mathbf{L^2})]^{2+}$, absorption spectra, cyclic voltammograms for all complexes, and additional crystallographic, spectroscopic, and catalytic data.

Acknowledgments

This work was supported by the Laboratory Directed Research and Development program at Pacific Northwest National Laboratory (PNNL). M. T. M. was supported as part of the Center for Molecular Electrocatalysis, an Energy Frontier Research Center funded by the U.S. Department of Energy, Office of Science, Office of Basic Energy Sciences. PNNL is operated by Battelle for the US Department of Energy.

[1] a) J. S. Kanady, E. Y. Tsui, M. W. Day, T. Agapie, *Science* **2011**, *333*, 733–736; b) J. Limburg, J. S. Vrettos, L. M. Liable-Sands, A. L. Rheingold, R. H. Crabtree, G. W. Brudvig, *Science* **1999**, *283*, 1524–1527.
[2] a) G. Berggren, M. F. Anderlund, S. Styring, A. Thapper, *Inorg. Chem.* **2012**, *51*, 2332–2337; b) R. Brimblecombe, A. Koo, G. C. Dismukes, G. F. Swiegers, L. Spiccia, *J. Am. Chem. Soc.* **2010**, *132*, 2892–2894; c) R. Sarma, A. M. Angeles-Boza, D. W. Brinkley, J. P. Roth, *J. Am. Chem. Soc.* **2012**, *134*, 15371–15386; d) H. Goff, R. K. Murmann, *J. Am. Chem. Soc.* **1971**, *93*, 6058–6065.
[3] S. M. Barnett, K. I. Goldberg, J. M. Mayer, *Nat. Chem.* **2012**, *4*, 498–502.
[4] J. L. Fillol, Z. Codolà, I. Garcia-Bosch, L. Gómez, J. J. Pla, M. Costas, *Nat. Chem.* **2011**, *3*, 807–813.
[5] A. L. Ward, L. Elbaz, J. B. Kerr, J. Arnold, *Inorg. Chem.* **2012**, *51*, 4694–4706.
[6] a) M. L. Helm, M. P. Stewart, R. M. Bullock, M. Rakowski DuBois, D. L. DuBois, *Science* **2011**, *333*, 863–866; b) M. O'Hagan, W. J. Shaw, S. Raugei, S. Chen, J. Y. Yang, U. J. Kilgore, D. L. DuBois, R. M. Bullock, *J. Am. Chem. Soc.* **2011**, *133*, 14301–14312; c) J. Y. Yang, R. M. Bullock, W. J. Shaw, B. Twamley, K. Fraze, M. Rakowski DuBois, D. L. DuBois, *J. Am. Chem. Soc.* **2009**, *131*, 5935–5945.
[7] C. T. Carver, B. D. Matson, J. M. Mayer, *J. Am. Chem. Soc.* **2012**, *134*, 5444–5447.
[8] J. L. Boyer, D. E. Polyansky, D. J. Szalda, R. Zong, R. P. Thummel, E. Fujita, *Angew. Chem.* **2011**, *123*, 12808; *Angew. Chem. Int. Ed.* **2011**, *50*, 12600–12604.
[9] H. Yamazaki, T. Hakamata, M. Komi, M. Yagi, *J. Am. Chem. Soc.* **2011**, *133*, 8846–8849.
[10] Z. Chen, J. J. Concepcion, X. Hu, W. Yang, P. G. Hoertz, T. J. Meyer, *Proc. Natl. Acad. Sci. USA* **2010**, *107*, 7225–7229.
[11] A. R. Parent, T. P. Brewster, W. De Wolf, R. H. Crabtree, G. W. Brudvig, *Inorg. Chem.* **2012**, *51*, 6147–6152.
[12] L. Duan, F. Bozoglian, S. Mandal, B. Stewart, T. Privalov, A. Llobet, L. Sun, *Nat. Chem.* **2012**, *4*, 418–423.
[13] a) M. Z. Ertem, L. Gagliardi, C. J. Cramer, *Chem. Sci.* **2012**, *3*, 1293–1299; b) W. C. Ellis, N. D. McDaniel, S. Bernhard, T. J. Collins, *J. Am. Chem. Soc.* **2010**, *132*, 10990–10991.
[14] C. J. Gagliardi, A. K. Vannucci, J. J. Concepcion, Z. Chen, T. J. Meyer, *Energy Environ. Sci.* **2012**, *5*, 7704–7717.
[15] a) S. E. Ghachtouli, R. Guillot, P. Dorlet, E. Anxolabehere-Mallart, A. Aukauloo, *Dalton Trans.* **2012**, *41*, 1675–1677; b) M. Martinho, G. Blain, F. Banse, *Dalton Trans.* **2010**, *39*, 1630–1634.
[16] C. M. Coates, K. Hagan, C. A. Mitchell, J. D. Gorden, C. R. Goldsmith, *Dalton Trans.* **2011**, *40*, 4048–4058.
[17] A. Draksharapu, Q. Li, H. Logtenberg, T. A. van den Berg, A. Meetsma, J. S. Killeen, B. L. Feringa, R. Hage, G. Roelfes, W. R. Browne, *Inorg. Chem.* **2011**, *50*, 900–913.
[18] A. M. Appel, S.-J. Lee, J. A. Franz, D. L. DuBois, M. Rakowski DuBois, B. Twamley, *Organometallics* **2009**, *28*, 749–754.
[19] I. Kaljurand, A. Kütt, L. Sooväli, T. Rodima, V. Mäemets, I. Leito, I. A. Koppel, *J. Org. Chem.* **2005**, *70*, 1019–1028.
[20] M. Costas, J. L. Que, *Angew. Chem.* **2002**, *114*, 2283; *Angew. Chem. Int. Ed.* **2002**, *41*, 2179–2181.

[21] M. J. Collins, K. Ray, L. Que, *Inorg. Chem.* **2006**, *45*, 8009–8011.
[22] I. Pecht, Z. Luz, *J. Am. Chem. Soc.* **1965**, *87*, 4068–4072.
[23] J. E. O'Reilly, *BBA-Bioenergetics* **1973**, *292*, 509–515.
[24] B. R. Galan, J. Schoffel, J. C. Linehan, C. Seu, A. M. Appel, J. A. S. Roberts, M. L. Helm, U. J. Kilgore, J. Y. Yang, D. L. DuBois, C. P. Kubiak, *J. Am. Chem. Soc.* **2011**, *133*, 12767–12779.
[25] a) D. F. Evans, *J. Chem. Soc.* **1959**, 2003; b) E. M. Schubert, *J. Chem. Educ.* **1992**, *69*, 62; c) D. H. Grant, *J. Chem. Educ.* **1995**, *72*, 39.

Received: December 12, 2012
Published Online: ■

Water-Oxidation Catalysis

Keywords: Homogeneous catalysis / Water splitting / Iron / Ligand effects / Proton transport

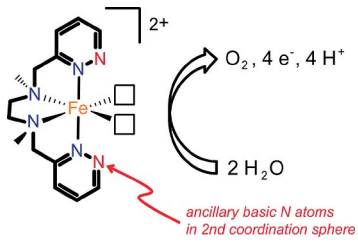

The structural, electrochemical, and catalytic properties of a family of iron-containing homogeneous water oxidation catalysts with pendant heteroatoms are studied. Slightly faster O_2 evolution relative to a parent compound is observed when the solvent pH is matched to the pK_a of the pendant nitrogen base, which might be attributable to interactions with substrate water.

